Chemical Engineering Journal 506 (2025) 160191

Contents lists available at ScienceDirect

Chemical Engineering Journal

journal homepage: www.elsevier.com/locate/cej

Enhancing SO_2 resistance in vanadium catalysts with tungsten disulfide for NH_3-SCR

Donghyeok Kim [a,b], Myeung-Jin Lee [a,b], Yejin Choi [a], Jongkyoung Kim [b], Bora Jeong [a], Bora Ye [a], Seungho Cho [b,*], Hong-Dae Kim [a,*]

[a] Green Materials & Processes R&D Group, Korea Institute of Industrial Technology, Ulsan 44413 Republic of Korea
[b] Department of Materials Science and Engineering, Ulsan National Institute of Science and Technology, Ulsan 44419 Republic of Korea

ARTICLE INFO

Keywords:
NH_3-SCR
SO_2-resistance
Tungsten disulfide
Sulfur vacancy
In-situ DRIFTS

ABSTRACT

NO_x emissions are a major environmental issue, and NH_3-SCR is a key method for their control. V-based catalysts perform well at high temperatures; however, SO_2-poisoning remains a critical issue for NH_3-SCR catalysts under low-temperature conditions. In this study, we develop an effective strategy of loading a stable sulfide two-dimensional (2D) material, WS_2, to enhance the SO_2 resistance of existing commercial V/Ti catalysts. In-situ DRIFTS analysis and spent SO_2-poisoning catalyst analyses are conducted to clarify the enhanced SO_2 resistance mechanism. These findings demonstrate that the superior SO_2 resistance can be attributed to the suppression of SO_2 by WS_2. Therefore, WS_2 loading inhibits the SO_2 adsorption and protects the NH_3 species adsorption, thereby enhancing the SO_2 resistance and low-temperature activity. This research can be utilized without changing the catalyst synthesis process, allowing it to be applied to current commercial catalysts, thereby underscoring its remarkable potential for industrial applications.

1. Introduction

Nitrogen oxide (NO_x) discharged from automotive and stationary sources is a severe environmental issue. The selective catalytic reduction of NH_3 (NH_3-SCR) is the most widely used and effective method for NO_x-emission control [1]. V-based catalysts are widely utilized in the thermal power stations owing to their high nitrogen selectivity and strong sulfur-poisoning resistance at high temperatures of 300–400 °C [2,3,4]. However, their activity and sulfur-poisoning resistance diminish at low temperatures below 250 °C, which hinders their application in treating low-temperature flue gasses [5]. Despite significant advances in developing sulfur-resistant catalysts, sulfur poisoning remains a challenge, as it gradually changes the physiochemical properties, leading to long-term catalyst degradation [6,7,8]. Consequently, improving the performance and SO_2 resistance of V-based catalysts at low temperatures remains a key challenge in NH_3-SCR research [9,10].

Generally, NH_3-SCR catalysts are poisoned by SO_2 through a three-steps process: (1) SO_2 is adsorbed onto the catalyst; (2) SO_2 is then oxidized to SO_3; and (3) this lead to the formation of ammonium sulfate (AS, $(NH_4)_2SO_4$), ammonium bisulfate (ABS, $(NH_4)HSO_4$), or metal sulfates, which can block and destroy the active sites of the catalyst [11]. Numerous studies have focused on increasing the SO_2 resistance in SCR catalysts through surface modifications. For example, metal promoters, such as Fe, W, and Ce, have been introduced to protect the main catalyst by allowing them to become poisoned instead [12,13]. However, such strategies encounter a problem: once the promoter is fully poisoned, the main catalyst also becomes poisoned, which decreases the sulfur resistance. Therefore, recent approaches have focused on increasing the SO_2 resistance by suppressing SO_2 adsorption, which is a prerequisite step in the SO_2-poisoning mechanism, using methods such as pre-coating the catalyst surface with sulfur [14]. Pre-sulfurization of the support or main catalyst material has typically been used as a strategy to inhibit SO_2 adsorption [15,16]. The pre-sulfurized catalyst showed slightly decreased activity, which was attributed to a lower specific surface area and relative scarcity of active sites. However, the increased SO_2 resistance resulted in a higher overall activity under SO_2 conditions. These

Abbreviations: NH_3-SCR, selective catalytic reduction of NO_x by NH_3; AS, ammonium sulfate; ABS, ammonium bisulfate; In-situ DRIFTS, in-situ diffuse reflectance infrared Fourier transform spectroscopy; XPS, X-ray photoelectron spectroscopy; XRD, X-ray diffraction; EDS, energy-dispersive X-ray spectroscopy; GHSV, gas hourly space velocity.

* Corresponding authors.
E-mail addresses: scho@unist.ac.kr (S. Cho), hdkim@kitech.re.kr (H.-D. Kim).

https://doi.org/10.1016/j.cej.2025.160191
Received 4 October 2024; Received in revised form 20 January 2025; Accepted 1 February 2025
Available online 4 February 2025

recent studies on enhancing SO_2 resistance share a common approach, in which sulfur atoms are loaded onto the surface in advance to suppress SO_2 adsorption.

In this study, a V_2O_5-WS_2/TiO_2 (denoted as VWS_2/Ti) catalyst for the NH_3-SCR was prepared using a simple wet-impregnation method, and to the best of our knowledge, the use of WS_2 in the NH_3-SCR field is a novel approach. WS_2 has a sulfur layer on the basal plane, allowing surface sulfur coating without the need for additional synthesis processes [17]. The basal plane of WS_2 contains a stable sulfide layer, which inhibits SO_2 adsorption. By inhibiting SO_2 adsorption, the NH_3 adsorption sites are protected, leading to improved SO_2 resistance. In addition, the W in WS_2 can replace tungsten oxide, which is a well-known promoter of V-based catalysts. In addition, WS_2 shows outstanding NH_3 adsorption capacity, and owing to its 2D characteristics, the main catalyst material promotes a high dispersion of V [18]. Furthermore, the synthesis method for the commercial V_2O_5-WO_3/TiO_2 (denoted as VW/Ti) catalyst remains unchanged, with the only modification being the replacement of the promoter material with WS_2. As previously mentioned, enhancing the SO_2 resistance through pre-sulfurization has the drawback of decreasing the number of active sites. To overcome this limitation, WS_2 with active sites mainly at the edge was annealed in a hydrogen atmosphere to increase the number of active sites on the basal plane, resulting in enhanced low-temperature activity [19]. Consequently, the improved performance at low temperatures and enhanced SO_2 resistance is observed for the VWS_2/Ti catalyst. Through comprehensive in-situ diffuse reflectance infrared Fourier transform spectroscopy (in-situ DRIFTS) and X-ray photoelectron spectroscopy (XPS) analyses, the corresponding NH_3-SCR reaction mechanism and SO_2 resistance enhancement effect are revealed in depth. Our study is noteworthy for industrial applications as the catalysts improve SO_2 resistance and low-temperature activity without substantial modifications to existing synthesis processes.

2. Material and methods

2.1. Catalyst preparation

A wet-impregnation method was employed to synthesize V/Ti and VWS_2/Ti. TiO_2 (DT-51, Cristal Global) was used as a support. For VWS_2/Ti catalyst, Ammonium metavanadate (NH_4VO_3, Daejung) was prepared at 2 wt% relative to the total catalyst weight and dissolved in EtOH with oxalic acid ($(COOH)_2$, Sigma-Aldrich) by stirring for 1 h. Tungsten disulfide (WS_2, Sigma-Aldrich), calculated at 7 wt%, was dissolved in EtOH and ultrasonicated for 1 h. The two solutions were mixed for 1 h before being impregnated onto a TiO_2 support, which was dissolved in EtOH. For V/Ti, the V solution was directly impregnated into the TiO_2 support solution. The resulting mixture was dried using an oil bath and then finely ground. The finely ground powder was calcinated at 400 °C for 2 h in air atmosphere. WS_2 was annealed at 500 °C in a hydrogen atmosphere under a 5 % H_2/Ar gas flow at 100 sccm for 2 h to create sulfur defects. The annealed sample in hydrogen condition was denoted as WS_2(H). The VWS_2/Ti catalyst synthesized using WS_2(H) was denoted as VWS_2/Ti(H).

2.2. Catalyst poisoning test

An SO_2-poisoning test was conducted to demonstrate the mechanism of enhanced SO_2 resistance by WS_2 loading. SO_2-poisoning is accelerated by the formation of AS and ABS. Thus, we conducted catalyst-poisoning experiments using two different methods under harsh SO_2 conditions to investigate the differences in their formation. In the first poisoning condition, SO_2-poisoning was performed with 1000 ppm NO, 1000 ppm SO_2, and 10 vol% H_2O under NH_3-free conditions to prevent the formation of AS and ABS species. The postfix notation S1 indicates that poisoning occurred under these conditions. Second, SO_2-poisoning was conducted using 1000 ppm NO, 1000 ppm NH_3, 1000 ppm SO_2, and 10 vol% H_2O due to formation of AS and ABS species. The catalysts poisoned under these conditions are labeled with the postfix S2.

2.3. Characterization

X-ray diffraction (XRD; Bruker AXS, D8 Advance) patterns were collected to investigate the crystal structures of the catalysts. Electron paramagnetic resonance spectroscopy (EPR; Bruker, EMX Plus) was used to demonstrate the possible sulfur vacancies. Raman spectroscopy (WITec, Alpha 300R) was used to characterize the chemical bond structures of the V and Ti species on the catalyst surface. Transmission electron microscopy equipped with an energy-dispersive X-ray spectroscopy (EDS) attachment (TEM; JEOL, JEM-2100F) was used to observe the micromorphology of the catalyst. The surface chemical states of the catalysts were detected by XPS (ThermoFisher, K-alpha) with an Al Kα X-ray radiation source. The elemental composition was determined by inductively coupled plasma optical emission spectroscopy (ICP-OES; Varian, 700-ES). X-ray fluorescence (XRF; PANalytical, Zetium) was used to quantitatively analyze the sulfur defects in WS_2.

Temperature-programmed desorption of NH_3 (NH_3-TPD) and temperature-programmed reduction of hydrogen (H_2-TPR) were conducted using a chemisorption analyzer (Micromeritics Instrument Corp., AutoChem II 2920). In-situ diffuse reflectance infrared Fourier transform spectroscopy (In-situ DRIFTS) experiments were performed using a Fourier transform infrared spectrometer (FT-IR; Bruker, Vertex 80v) equipped with a Harrick DRIFT cell and liquid nitrogen-cooled mercury cadmium telluride (MCT) detector. Prior to each experiment, the sample was pretreated under each test condition for 60 min under an N_2 flow of 300 sccm. The background spectrum was collected in the flow of N_2 after pretreatment and automatically subtracted from the sample spectrum for each test.

2.4. Catalytic performance evaluation

The NO_x removal efficiency was evaluated using a fixed-bed reactor with an inner diameter of 12.7 mm and a length of 400 mm. The NH_3-SCR activity was measured under the following conditions: 300 ppm NO, 300 ppm NH_3, 300 ppm SO_2 (when used), and 5 % O_2 with an N_2 balance. The total flow rate was 500 mL min^{-1}, and 0.5 mL of the prepared powder was used. Thus, the gas hourly space velocity (GHSV) was 60,000 h^{-1}. The measurement was conducted in the temperature range of 150–400 °C at intervals of 50 °C, and each temperature point was stabilized for 30 min. The gas concentrations at the inlet and outlet were analyzed using gas-phase Fourier transform infrared spectroscopy (FT-IR; Gasmet, CX-4000). In addition, the O_2 concentration was determined using an O_2 analyzer (Enotec, OXITEC 5000). The percentage of NO_x conversion and N_2 selectivity were calculated using Eq. (1) and (2), respectively.

$$\text{NO}_x\ \text{conversion}\ (\%) = \frac{[\text{NO}_x]_{in} - [\text{NO}_x]_{out}}{[\text{NO}_x]_{in}} \times 100\% \quad (1)$$

$$\text{N}_2\ \text{selectivity}\ (\%) = \left(1 - \frac{2 \times [\text{N}_2\text{O}]_{out} + [\text{NO}_2]_{out}}{[\text{NO}_x]_{in} + [\text{NH}_3]_{in} - [\text{NO}_x]_{out} - [\text{NH}_3]_{out}}\right) \times 100\% \quad (2)$$

Kinetic analysis methods details were described in supplementary information.

3. Results and discussion

3.1. Catalytic performance and SO_2 resistance

The NH_3-SCR performance, NO_x conversion, and SO_2/H_2O tolerance of the as-prepared catalysts were investigated to determine the influence of WS_2 on the NH_3-SCR performance of the V-based catalysts. Across all temperature ranges, the N_2 selectivity of all catalysts remained above 95

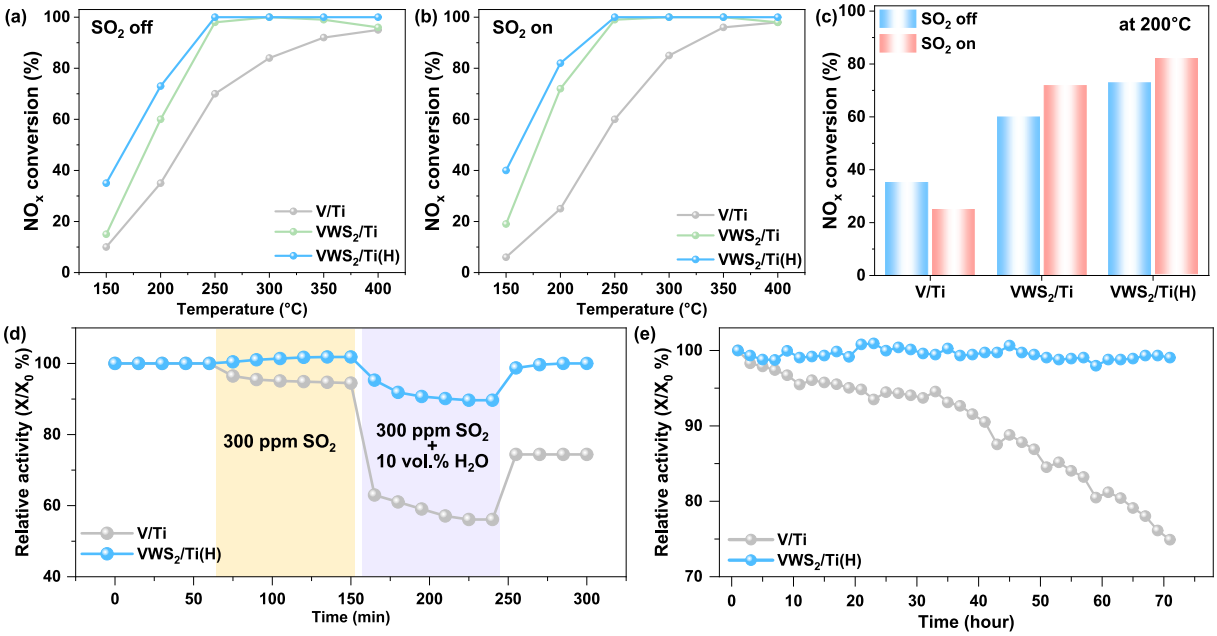

Fig. 1. Effect of the reaction temperature on the NO_x conversion of V/Ti, VWS_2/Ti, and VWS_2/Ti(H) both (a) without and (b) with SO_2. The test conditions were: 300 ppm NO, 300 ppm NH_3, 300 ppm SO_2 (when used), and 5 vol% O_2, balanced with N_2, and GHSV of 60,000 h^{-1}. (c) NO_x conversion depending on the presence and absence of SO_2. (d) Relative activity of the NO_x conversion for the effect on SO_2 and H_2O. The test conditions were: 300 ppm NO, 300 ppm NH_3, 300 ppm SO_2, 5 vol% O_2, and 10 vol% H_2O at 225 °C. (e) Relative activity of a long-term SO_2/H_2O resistance stability test. The corresponding actual activity is presented in Fig. S8. The test conditions were: 300 ppm NO, 300 ppm NH_3, 300 ppm SO_2, 5 vol% O_2, and 10 vol% H_2O at 225 °C.

% (Fig. S1). As shown in Fig. 1(a) and (b), the NH_3-SCR activities of V/Ti, VWS_2/Ti, and VWS_2/Ti(H) were evaluated at 150–400 °C without and with SO_2. The overall activity showed that loading WS_2 into the V/Ti catalyst enhanced the activity owing to the interaction between W and V, which further increased when additional active sites were introduced into WS_2. Experimental findings suggest that the ideal WS_2 loading is 7 wt% (Fig. S2 and Fig. S3). When SO_2 was injected, the activity usually decreased at temperatures below 250 °C, and the V/Ti

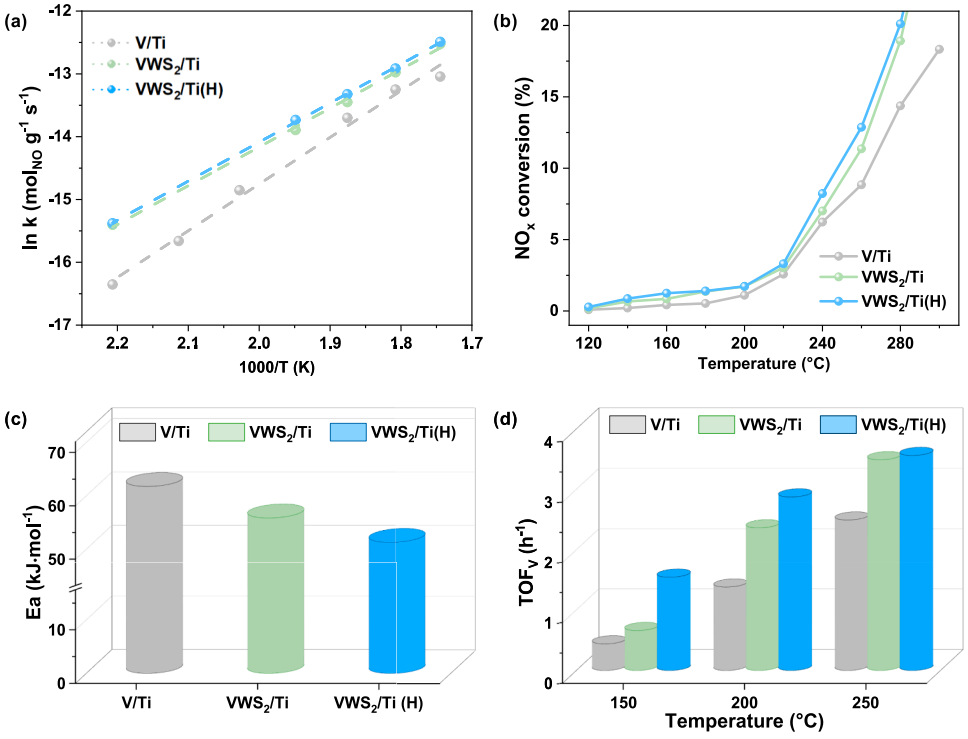

Fig. 2. Kinetic calculation results of Arrhenius plots (a), and the corresponding NO_x conversions (b) and activation energies (E_a) (c). The test conditions were: 300 ppm NO, 300 ppm NH_3, 300 ppm SO_2, and 5 vol% O_2. (d) Turnover frequency (TOF) calculated based on the corresponding information in Fig. 1(b).

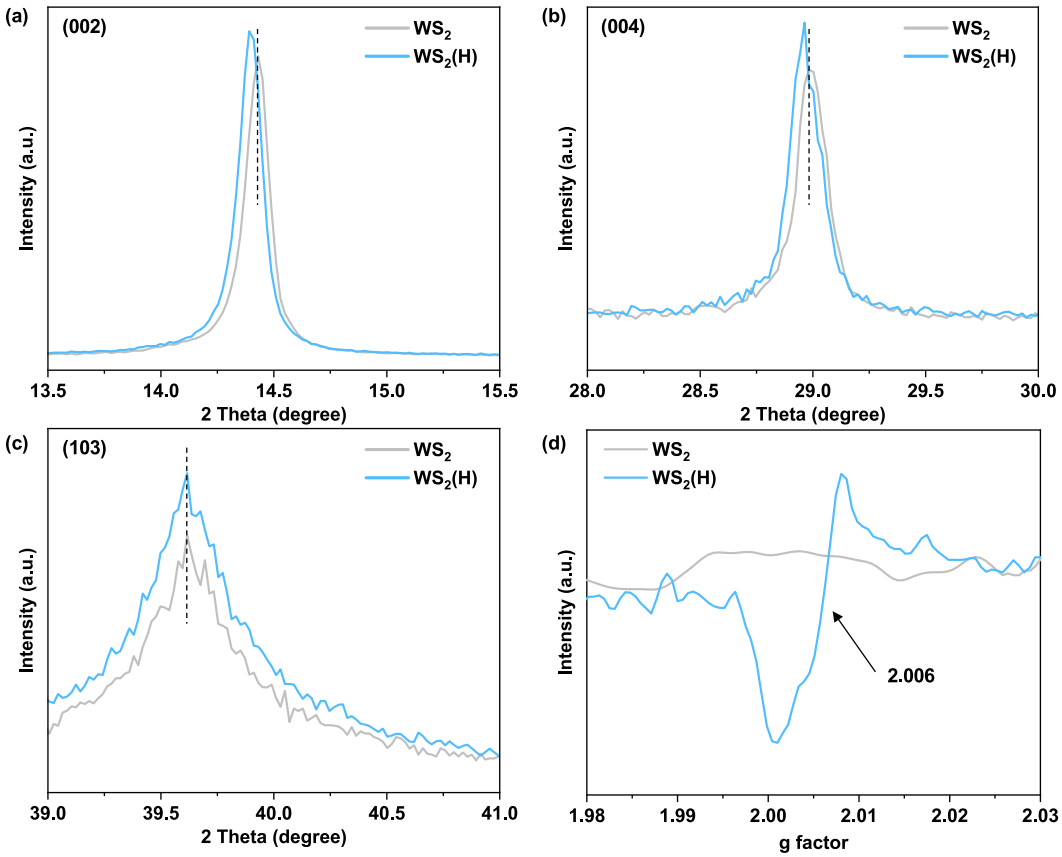

Fig. 3. XRD patterns (a–c) and EPR spectra (d) of pristine WS_2 and WS_2(H).

catalyst showed a corresponding decrease in activity. However, the catalysts loaded with WS_2 exhibited an increased activity, even in the presence of SO_2, across the entire temperature range. When comparing conditions with and without SO_2 at 200 °C, the V/Ti catalyst experienced a 10 % decreasing in activity, whereas the WS_2-loaded catalysts showed an approximately 10 % increase (Fig. 1(c)). Some studies have reported that the presence of SO_2 in NH_3-SCR reactions can enhance catalyst activity. For example, research using rare-earth based catalysts showed significant increase in SCR performance when SO_2 and H_2O were present simultaneously [20]. This was attributed to the formation of $S_2O_7^{2-}$ species on the catalyst surface, which provided additional acid sites and promoted the SCR reaction. Additionally, studies where sulfur was coated on the catalyst surface also showed an increase in activity. This behavior is considered to occur because SO_2 forms specific sulfate species on the catalyst surface, creating additional acid sites that improve the efficiency of the SCR reaction. We evaluated the applicability of WS_2 to other SCR catalysts, such as Mn and Cu catalysts (Fig. S4).

Additional evaluations were conducted to determine the difference between WS_2 and WO_3, well-known promoter for V/Ti commercial catalyst (Fig. S5). The activity evaluation results showed that under SO_2 off conditions, the activity of the VW/Ti catalyst was higher than the VWS_2/Ti catalyst but slightly lower than the VWS_2/Ti(H) catalyst. Both WO_3 and WS_2 contain tungsten, collaborates well with vanadium. However, the sulfur layer on the basal plane of WS_2 prevents the formation of dangling bonds, resulting in active sites are placed only at the edge sites. Therefore, WO_3, containing abundant oxygen vacancies and functional groups, demonstrates higher activity under SO_2 off conditions. To overcome this phenomenon, we introduced additional active sites on the basal plane of WS_2 through hydrogen condition annealing. As a result, the activity was indicated to be higher than the VW/Ti catalyst even under SO_2 off conditions. Furthermore, under SO_2 on conditions typical in actual industrial environments, the activity behavior is reversed. Although the activity of the VWS_2/Ti catalyst was lower under SO_2 off conditions, but superior SO_2 resistance resulted in higher activity compared to the VW/Ti catalyst under SO_2 on conditions.

The effect of WS_2 loading on the SO_2/H_2O resistance and long-term stability of the catalysts were evaluated, and the results are shown in Fig. 1(d) and (e). As previously mentioned, the VWS_2/Ti(H) catalyst displayed an increased activity when SO_2 was injected. Nevertheless, when both SO_2 and H_2O were present, the activities of both the V/Ti and VWS_2/Ti(H) catalysts decreased. The V/Ti catalysts exhibited a 44 % decrease in activity compared with the initial performance, whereas the VWS_2/Ti(H) catalyst exhibited only a 11 % decrease in activity. Cycle test was conducted on the VWS_2/Ti(H) catalyst to evaluate the activity impact of the spent sample (Fig. S6).

Long-term stability tests were conducted under the SO_2 (Fig. S7), and SO_2/H_2O conditions (Fig. 1(e)). In the presence of H_2O and SO_2, the VWS_2/Ti(H) catalyst showed a stable activity for three days after an initial decrease in activity. In contrast, the V/Ti catalyst exhibited a continuous decline in activity for three days after the initial decrease. These results demonstrated that the VWS_2/Ti(H) catalyst effectively improved the low-temperature activity and significantly enhanced the SO_2 resistance. These advantageous properties render the VWS_2/Ti(H) catalyst a promising candidate for practical industrial applications, particularly in the presence of H_2O and SO_2.

3.2. Kinetics analysis

The calculated Arrhenius plots and corresponding NO_x conversion results are presented in Fig. 2(a) and (b), respectively. Owing to the exclusion of thermal and diffusion effects at different temperatures, the NO_x conversion was determined to be lower than 20 % by testing under a GHSV of 4,000,000 h^{-1}. The reaction rate was closely related to the

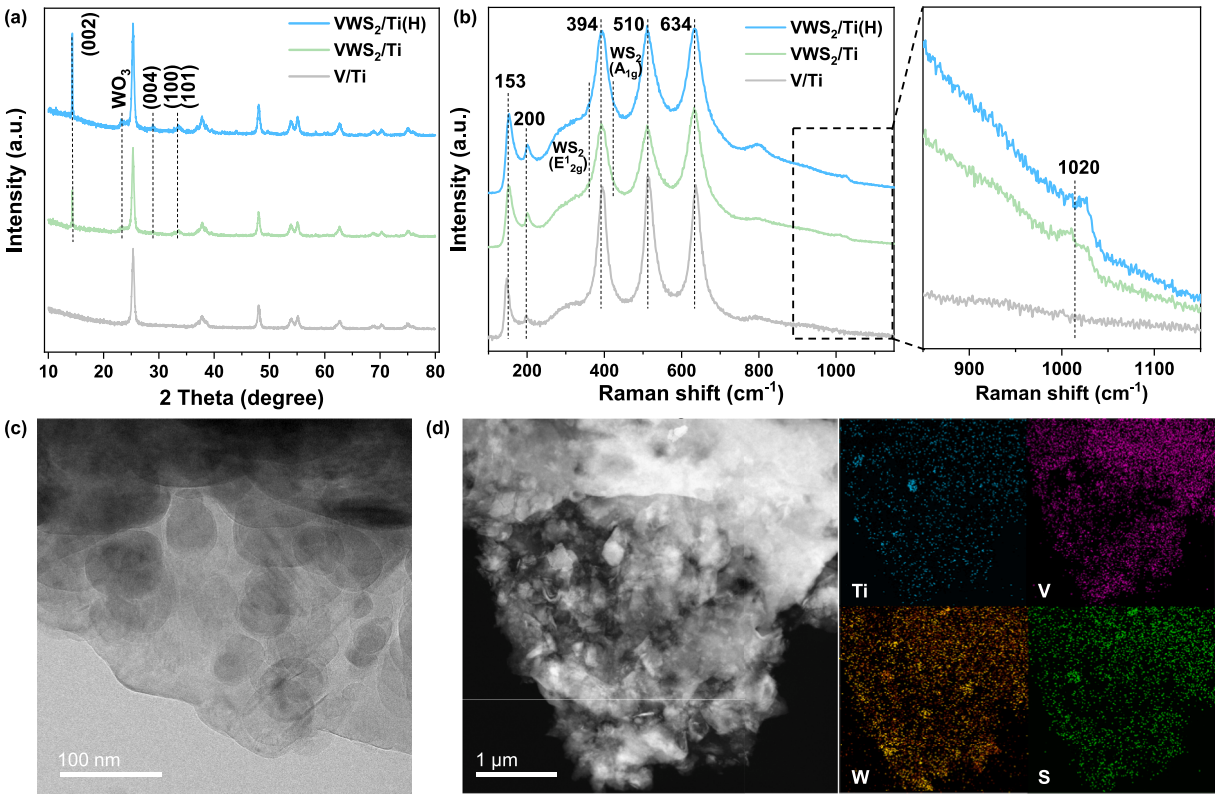

Fig. 4. XRD patterns (a) and Raman spectra (b) of V/Ti, VWS_2/Ti, and VWS_2/Ti(H) catalysts. HR-TEM image (c) and STEM-EDS mappings (d) of VWS_2/Ti(H).

activation energy, and the activation energy calculated from the slope of the Arrhenius plot is shown in Fig. 2(c). For the VWS_2/Ti(H), the activation energy (51.29 kJ mol^{-1}) was lower than those of V/Ti (61.77 kJ mol^{-1}) and VWS_2/Ti (55.87 kJ mol^{-1}). This indicated that the strong interaction between the W species of WS_2 and V species in the catalyst reduced the catalyst reaction activation energy, which further decreased when additional active sites were supplied on the basal plane of WS_2. WS_2 is a TMD material with a layered structure, is arranged in an S-W-S configuration. The basal plane consists of sulfur atoms bonded through stable covalent bonds, which eliminates dangling bonds and ensures chemical stability with low reactivity. In contrast, the edge site, a structurally incomplete region, exposes unbound sulfur or tungsten atoms. This asymmetric bonding forms dangling bonds, inducing electronic instability and enhancing reactivity. These characteristics make WS_2 edge sites widely utilized as active sites in catalysis. Therefore, reaction such as reactant adsorption are difficult to occur on the basal plane, making it ineffective as an active site. To address the problem, we created additional active sites by introducing sulfur vacancies. Active sites formed on the basal plane dedcreased the activation energy, and the effects were confirmed through simple DFT calculations (Fig. S9). The activation energy results further confirmed that the VWS_2/Ti(H) catalyst had the highest catalytic activity under an SO_2 atmosphere in the NH_3-SCR reaction.

The turnover frequency (TOF) was calculated to study the intrinsic activities of the catalysts, as shown in Fig. 2(d). The turnover frequency of the VWS_2/Ti(H) catalyst was consistently higher than that of V/Ti and slightly higher than that of VWS_2/Ti. This result was consistent with the activation energy obtained from the Arrhenius plot, indicating that the coexistence of V and WS_2 was beneficial for enhancing the activity of the catalyst under an SO_2 atmosphere.

3.3. Structural properties

Hydrogen annealing was applied to WS_2 due to enhance catalytic activity by generating sulfur vacancies on basal plane. The XRD spectra of pristine WS_2 and hydrogen-reduced WS_2 are presented in Fig. 3(a–c) and Fig. S10, respectively. All samples showed a 2H WS_2 structure. Fig. 3 (a–c) show magnified views of the (002), (004), and (103) diffraction peaks. The interlayer bonding of WS_2 was bound by weak van der Waals forces. The formation of sulfur vacancies weakened the interlayer bonding, leading to an increase in the d-spacing [19]. The peak positions of the (002) and (004) planes of the hydrogen-reduced WS_2 were shifted to a low θ. When the θ value was decreased, the d-spacing of the planes increased, indicating the formation of a sulfur vacancy. Conversely, the peak positions of the (103) plane remained unchanged (Fig. 3(c)), unlike the interlayer peak.

Fig. 3(d) shows the EPR spectra of pristine WS_2 and the reduced sample. Since there are usually only a few singly charged sulfur vacancies, the magnetization of these samples is small. The peak seen at a g-factor of approximately 2.006 was associated with the contribution of unpaired electron radicals because of generating sulfur vacancies in WS_2 (Fig. S11) [21]. A larger peak area and higher peak intensity implied a higher concentration of sulfur vacancies. To further confirm the formation of sulfur vacancies, quantitative analyses were performed using XRF and XPS (Table S1). Both results showed decrease in sulfur concentration, with the surface atomic concentration exhibiting greater reduction.

The results regarding the stability of WS_2 on the catalyst surface in H_2O condition after poisoning are presented in the XPS (Fig. 8) and XRD (Fig. S12) results. Although no structural changes were observed, for more detailed analysis, WS_2 alone was subjected to poisoning in H_2O and SO_2 condition at 300 °C and subsequently analyzed. Poisoning was conducted at 300 °C where 100 % activity is achieved to produce the spent sample and analyzed using XRD and SEM (Fig. S13). After poisoning at 300 °C, no changes were observed in the phase of WS_2 (Fig. S13(a)). Additionally, the morphology and mapping images showed no alterations (Figs. S13(b-d)), confirming the hydrothermal stability shows no concerns. To determine the thermal stability of WS_2,

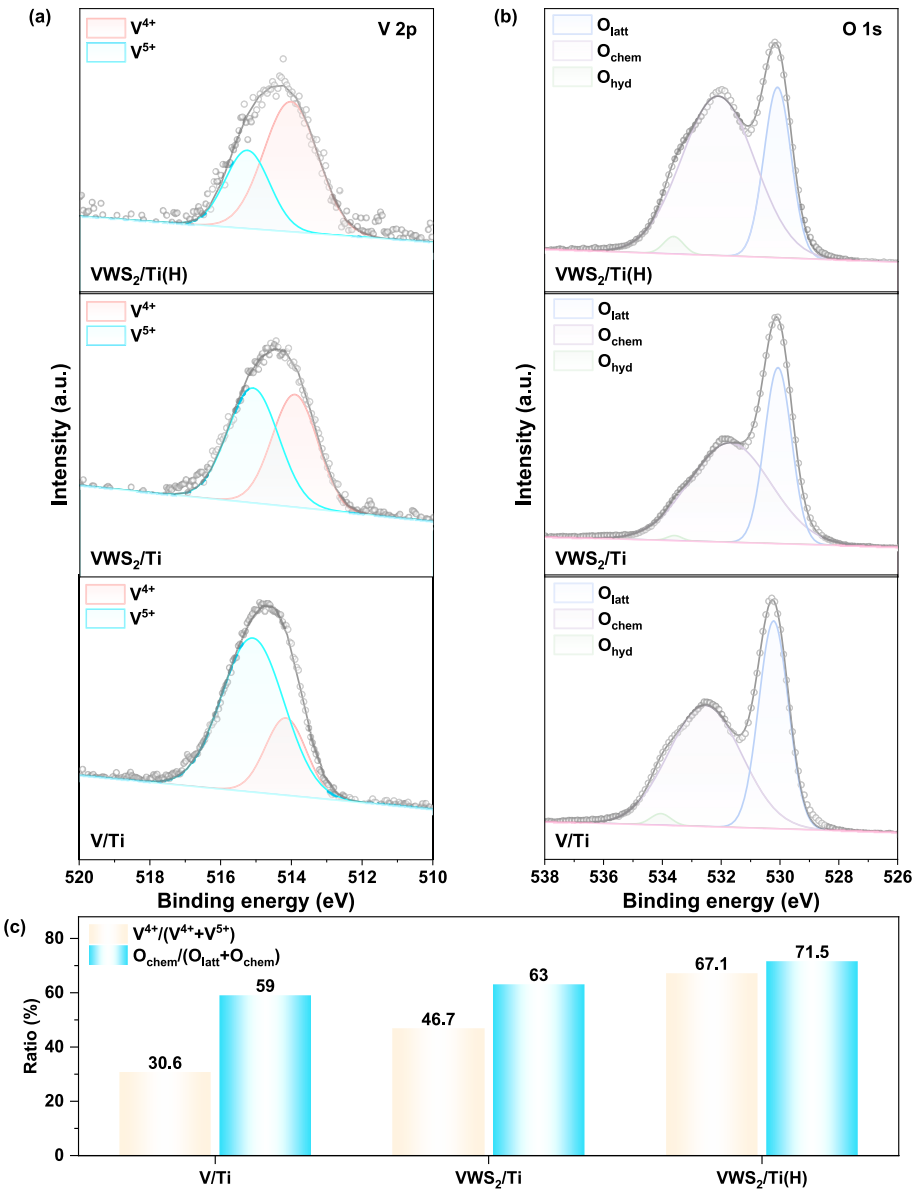

Fig. 5. XPS spectra of V 2p (a) and O 1s (b) of V/Ti, VWS_2/Ti, and VWS_2/Ti(H) catalysts, and a histogram of the valence states ratios of different elements (c).

annealing was performed at 400 °C on both WS_2 and WS_2(H) samples (Fig. S14). As shown in Fig. 3(a), slight oxidation of WS_2 to WO_3 was observed. However, the peak of WS_2 remained unchanged, confirming that the structure of WS_2 did not collapse. The WS_2(H) sample with defects exhibited slightly more oxidation compared to pristine WS_2. Nevertheless, since the catalyst achieves 100 % activity below 300 °C, calcination above 300 °C is unnecessary in industrial applications. At 300 °C, WS_2 does not begin to oxidize, suggesting that the stability is sufficient under these conditions.

The XRD patterns of the V/Ti, VWS_2/Ti, and VWS_2/Ti(H) catalysts are presented in Fig. 4(a), and all the samples showed a typical anatase-phase TiO_2 (ICDD 00-001-0562) structure. No diffraction peaks of V-related species, such as V_2O_5 (ICDD 00-001-0359) and VO_2 (ICDD 00-009-0142), were observed in any of the samples, suggesting that the V species were highly dispersed on the TiO_2 or that the particle size was smaller than the XRD limit of detection [22]. WS_2 crystals (ICDD 00-035-0651) were formed at 14.4°, 28.9°, and 33.6° on both the VWS_2/Ti and VWS_2/Ti(H) catalysts. Several small peaks assigned to the WO_3 crystal (ICDD 00-001-0486) were also observed in the XRD patterns at 23–24°, indicating that the WS_2 crystal was slightly oxidized when the catalyst was calcinated [23]. This indicates WS_2 was slightly oxidized to WO_3, as confirmed by the added Fig. S15, which shows the oxidation temperature of WS_2. Oxidation of WS_2 begins around 400 °C, and since the catalyst was calcinated at 400 °C for 2 h, the partial oxidation of WS_2 to WO_3 was also confirmed.

The crystal structures of the catalysts before and after the S2-poisoning test were further analyzed using XRD, and the results are presented in Fig. S12. The XRD patterns of all catalysts consistent after poisoning, suggesting that SO_2-poisoning did not lead to significant structural collapse of the catalysts.

Fig. 4(b) shows the Raman spectra acquired to investigate the effects of VO_x species on the WS_2 of the catalysts. For all catalysts, characteristic Raman bands at 153, 200, 394, 510, and 634 cm^{-1} corresponded to the anatase phase TiO_2. In the range of 850–1150 cm^{-1}, the band at 1020 cm^{-1} was attributed to the monomeric V=O vibration [24]. The absence of a crystalline V_2O_5 band at approximately 995 cm^{-1} confirmed that V_2O_5 particles were not present. The V=O band intensities of the VWS_2/Ti and VWS_2/Ti(H) catalysts were higher than those of the V/Ti catalyst, indicating that the V species were uniformly dispersed on the WS_2 (002) plane [25]. This result is also observable on the STEM-EDS mapping

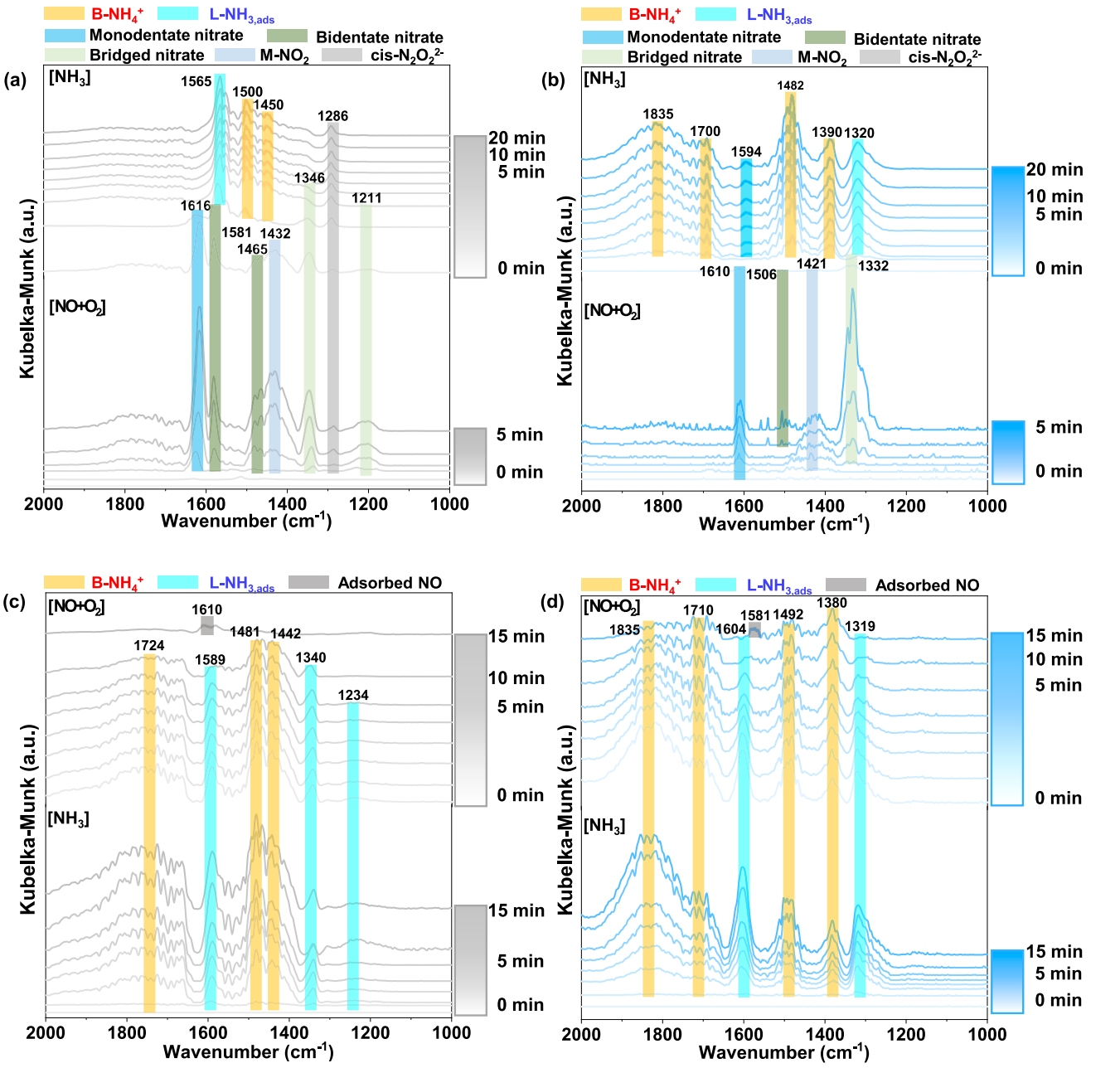

Fig. 6. In-situ DRIFTS spectra of 1000 ppm NH_3 with pre-adsorbed 1000 ppm NO + 5 vol% O_2 at 150 °C on V/Ti (a) and VWS_2/Ti(H) (b). In-situ DRIFTS spectra of 1000 ppm NO + 5 vol% O_2 with pre-adsorbed 1000 ppm NH_3 at 150 °C on V/Ti (c) and VWS_2/Ti(H) (d).

image in Fig. 4(d). The high-resolution TEM and STEM-EDS mapping images are presented in Fig. 4(c) and (d), respectively, on which uniformly dispersed TiO_2 and V species can be observed. The difference in dispersion can be clearly observed when compared to the V/Ti catalyst (Fig. S16).

3.4. Surface chemical environment analysis

The surface electronic states of the catalysts were investigated using XPS, and the corresponding fine spectra of V 2p and O 1s are shown in Fig. 5. The surface composition proportions and BET surface area are listed in Table S2 and Table S3, respectively. As shown in Fig. 5(a), V 2p peaks were clearly detected in all samples, where V^{5+} coexisted with V^{4+}. Compared with the V/Ti catalyst, a significant increase in the V^{4+} ratio was observed for the VWS_2/Ti and VWS_2/Ti(H) catalysts, as shown in Fig. 5(c). This suggested that the interaction between V and WS_2 reduced the oxidation state of V. The abundance of defective V^{4+} species improved the catalyst activity at low temperatures owing to the high redox capacity of the V^{4+} species [26,27]. This indicates the positive effect of WS_2 on the redox properties and the enhanced activity of VWS_2/Ti(H) at low temperatures owing to structural interactions.

The O 1s XPS profiles of the catalysts are shown in Fig. 5(b). The O 1s XPS spectra were fitted with three peaks, which were assigned as lattice oxygen species (529.7–230.1 eV, marked as O_{latt}), surface chemisorbed oxygen species (531.8–532.1 eV, marked as O_{chem}), and hydroxyl group oxygen species (533.4–533.8 eV, marked as O_{hyd}). The O_{chem} species were the most active oxygen species in the oxidation reactions owing to their higher mobility compared with that of the O_{latt} species [28]. As shown in Fig. 5(c), the relative concentration ratio of $O_{chem}/(O_{chem} + O_{latt})$ increased in the following order: V/Ti (59 %) < VWS_2/Ti (63 %) < VWS_2/Ti(H) (71.5 %), indicating that VWS_2/Ti(H) had the highest surface oxidative capability.

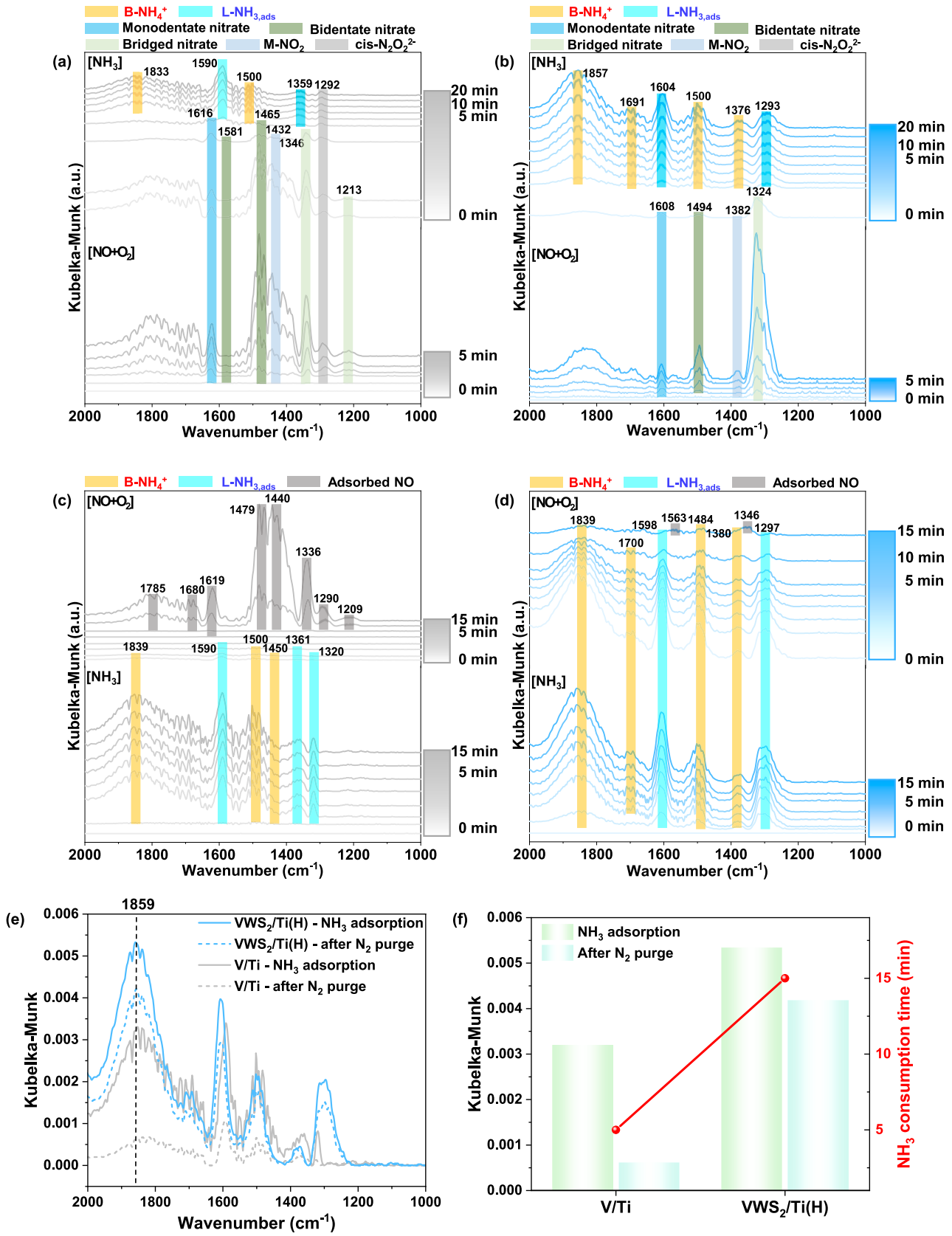

Fig. 7. In-situ DRIFTS spectra of 1000 ppm NH_3 with pre-adsorbed 1000 ppm NO + 5 vol% O_2 at 150 °C on V/Ti-S2 (a) and VWS_2/Ti(H)-S2 (b). In-situ DRIFTS spectra of 1000 ppm NO + 5 vol% O_2 with pre-adsorbed 1000 ppm NH_3 at 150 °C on V/Ti-S2 (c) and VWS_2/Ti(H)-S2 (d). (e) In-situ DRIFTS spectra of pre-adsorbed 1000 ppm NH_3 for 15 min, and the spectra after a 3-min N_2 purge on V/Ti-S2 and VWS_2/Ti(H)-S2. (f) The NH_3 adsorption intensity at 1859 cm^{-1} and pre-adsorbed NH_3 consumption time of V/Ti-S2 and VWS_2/Ti(H)-S2.

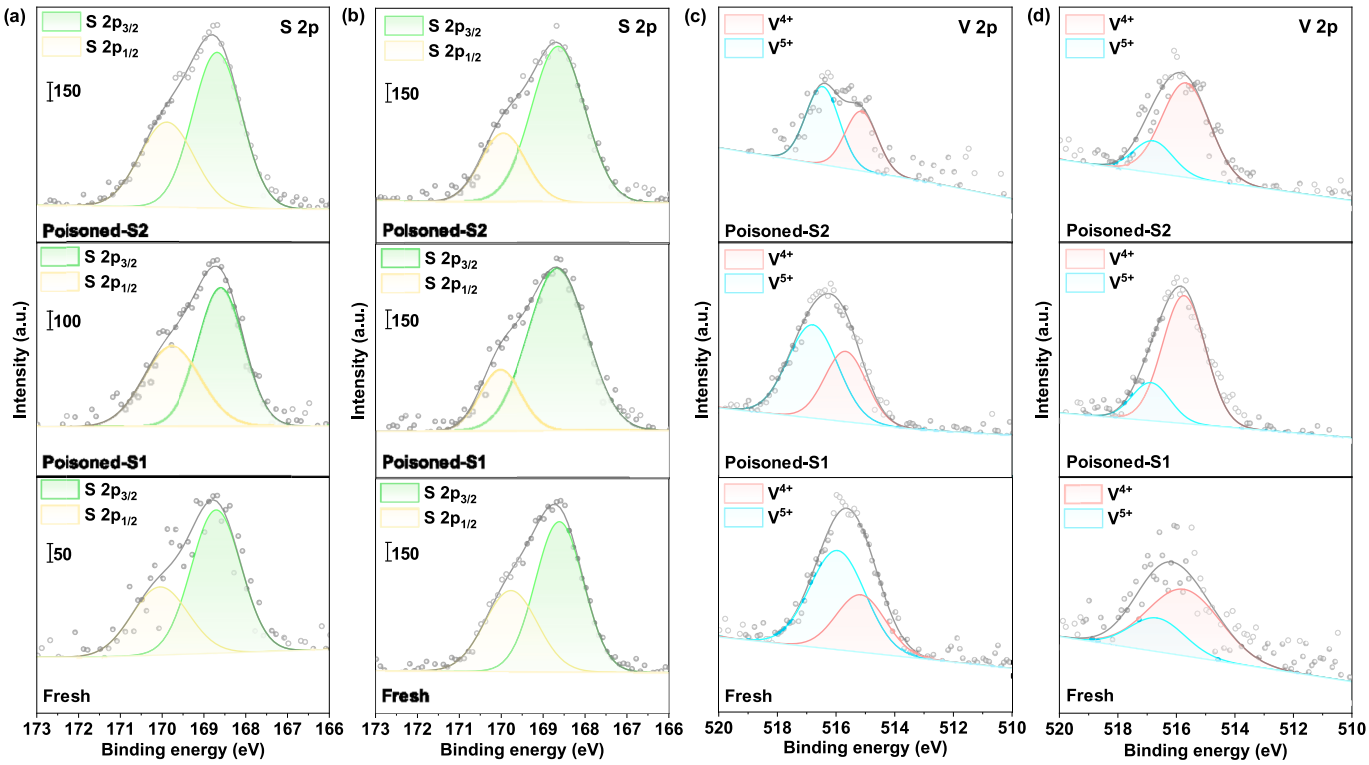

Fig. 8. XPS profiles of fresh, S1-poisoned, and S2-poisoned catalysts of S 2p on V/Ti (a) and VWS_2/Ti(H) (b), and V 2p on V/Ti (c) and VWS_2/Ti(H) (d).

3.5. *In-situ DRIFTS: Reaction mechanism study*

To investigate the reaction mechanism of the NH_3-SCR, the adsorption behavior of the reactants on the catalyst surface and reaction process were studied using in-situ DRIFTS. Competitive adsorption experiments were conducted on all catalysts, where NH_3 was adsorbed onto surfaces with pre-adsorbed NO + O_2, and vice versa, with NO + O_2 adsorbed onto surfaces with pre-adsorbed NH_3. In addition, the samples pretreated with S2-poisoning condition were evaluated following the same in-situ DRIFTS gas injection sequences to determine the reasons for the increased SO_2 resistance.

3.5.1. *Reactant adsorption and desorption behaviors of catalysts*

In-situ DRIFTS spectra for 1000 ppm NH_3 adsorption with pre-adsorbed 1000 ppm NO + 5 vol% O_2 at 150 °C on the V/Ti and VWS_2/Ti(H) catalysts is presented in Fig. 6(a–d). The majority of adsorption occurred in the form of nitrates for both V/Ti and VWS_2/Ti (H) catalysts. The main adsorbed species of NO included monodentate nitrate linked to Ti sites (~1616 cm^{-1}), bidentate nitrate linked to Ti sites (1450–1581 cm^{-1}), and bridged nitrate (~1346 and ~1211 cm^{-1}) [29]. M−NO_2 species (~1432 cm^{-1}), which promoted fast-SCR, were adsorbed on both catalysts and rapidly consumed for reaction. The band located at 1286 cm^{-1} for the V/Ti catalyst was assigned to *cis*-$N_2O_2^{2-}$ [30]. The *cis*-$N_2O_2^{2-}$ species were adsorbed with relatively good stability on the catalyst surface, indicating that *cis*-$N_2O_2^{2-}$ species were difficult to react with NH_3. Indeed, the *cis*-$N_2O_2^{2-}$ species was still present after adsorbing NH_3 for 20 min in Fig. 6(a). With the formation of the pre-adsorbed nitrate species, the subsequently adsorbed NH_3 reacted without creating a separate NH_3 adsorption peak, leading to the consumption of the nitrate species. The observation of the NH_3 adsorption peak after the reaction with the adsorbed nitrate species on both catalysts was in accordance with the L–H mechanism [31]. The consumption time of pre-adsorbed NO species was 4 and 1 min for the V/Ti and VWS_2/Ti(H) catalysts, respectively, indicating that the reaction rate of the VWS_2/Ti(H) catalyst was faster than that of the V/Ti catalyst.

The in-situ DRIFTS spectra of the 1000 ppm NO + 5 vol% O_2 adsorption with pre-adsorbed 1000 ppm NH_3 at 150 °C on V/Ti and VWS_2/Ti(H) are collected in Fig. 6(c) and (d), respectively. With the progression of adsorption time, the bands at 1380, 1442, 1481, 1492, 1710, 1724, and 1835 cm^{-1} were assigned to the bending vibration of the NH_4^+ species on Brønsted acid sites[30,32]. The bands at 1234, 1319, 1589, and 1604 cm^{-1} were ascribed to the bending vibration of the N—H bonds in NH_3 linked to a Lewis acid site [33,34,35]. The absence of the adsorbed NO peak before the reaction was completed with the NH_3 species on both catalysts indicated that the decrease in NH_3 species might have resulted from the reaction between the adsorbed NH_3 and gas-phase NO species. This result was consistent with the E–R mechanism [36]. NH_3 species were more likely adsorbed on the Lewis acid site on the V/Ti catalyst at 150 °C to form a large amount of NH_3, while NH_4^+ tended to be adsorbed on the Brønsted acid sites on the VWS_2/Ti(H) catalyst. Consequently, the relatively large amount of easily desorbed weak Brønsted acid sites contributed to the high activity of VWS_2/Ti(H) at low temperatures [37,38]. The increased amount of Brønsted acid sites on the VWS_2/Ti(H) catalyst was also confirmed by the in-situ DRIFTS spectra of NH_3 adsorption at 50 °C (Fig. S17) and NH_3-TPD (Fig. S18 and Table S4).

To investigate the enhanced adsorption of NH_3 upon loading WS_2 onto the catalyst, in-situ DRIFTS analyses on the individual components of the VWS_2/Ti(H) catalyst were conducted, as presented in Fig. S19. First, the support material TiO_2, with its large surface area, adsorbed significant amounts of both the NH_3 and NO species. Conversely, the active catalytic material V_2O_5 exhibited minimal adsorption of both the NH_3 and NO species. WS_2 adsorbed NO species poorly, whereas NH_3 species were effectively adsorbed. This property caused the additional NH_3 adsorption sites on the VWS_2/Ti(H) catalyst.

3.5.2. *Reactant adsorption and desorption behaviors of poisoned catalysts*

To study the effect of ABS formation on the catalyst surface in the NH_3-SCR mechanism, an in-situ DRIFTS analysis was conducted on samples poisoned under S2 conditions. In-situ DRIFTS spectra of 1000

Table 1
Surface atomic ratios of sulfur, relative atomic ratio of V species, and reducible property for each catalyst.

Samples	Surface atomic ratio[a]	Relative atomic ratio[a]	Reducible property[b]
	Sulfur (%)	$V^{4+}/(V^{4+}+V^{5+})$ (%)	H_2 consumption (mmol g_{cat}^{-1})
V/Ti	4.04	30.62	0.76
V/Ti-S1	5.21	38.58	0.81
V/Ti-S2	13.22	42.29	0.98
VWS_2/Ti(H)	13.47	67.13	1.67
VWS_2/Ti(H)-S1	13.7	74.32	1.69
VWS_2/Ti(H)-S2	14.79	74.45	1.70

[a] via XPS.
[b] via H_2-TPR.

ppm NH_3 adsorption with pre-adsorbed 1000 ppm NO + 5 vol% O_2 at 150 °C on the V/Ti-S2 and VWS_2/Ti(H)-S2 catalysts is presented in Fig. 7 (a) and (b), respectively. For the pre-adsorbed NO species, the NO adsorption species appeared identical to the adsorption species on the fresh catalyst.

The in-situ DRIFTS spectra of the 1000 ppm NO + 5 vol% O_2 adsorption with pre-adsorbed 1000 ppm NH_3 at 150 °C on V/Ti-S2 and VWS_2/Ti(H)-S2 are presented in Fig. 7(c) and (d), respectively. As shown in Fig. 7(d), the NH_3 adsorption species on VWS_2/Ti(H)-S2 were identical to the adsorption species on the fresh catalyst. In the case of the V/Ti catalyst, the NH_3 adsorption sites were similar to those of the fresh catalyst, but a noticeable decrease in the intensity of the Brønsted acid sites at 1450 and 1500 cm^{-1} was confirmed. The NH_3 adsorption intensity was compared for 15 min with the intensity after N_2 purging for 3 min, as depicted in Fig. 7(e) and (f). The peak observed at 1859 cm^{-1} in the Fig. 7(e) corresponds to a Brønsted acid site, which serves a crucial role in the SCR reaction and is utilized to calculate the adsorption strength. Notably, after N_2 purging for 3 min, the NH_3 adsorption intensity decreased significantly by 81 % compared with that after NH_3 adsorption for 15 min with V/Ti-S2. This was because ABS formation on the V/Ti catalyst surface blocked the active sites, thereby suppressing NH_3 chemical adsorption on the catalyst surface and resulting in physical adsorption. However, the intensity of the VWS_2/Ti(H)-S2 peak decreased by only 21 %, suggesting that WS_2 protected the NH_3 adsorption sites by suppressing SO_2 adsorption. The decreased values for all peaks are presented in Fig. S20.

Consequently, the VWS_2/Ti(H)-S2 catalyst could chemically adsorb more NH_3, leading to a longer reaction time for the pre-adsorbed NH_3 with NO than that of the V/Ti-S2 catalyst, as shown in Fig. 7(f).

3.6. Exploration of poisoned catalysts

3.6.1. Surface chemical environment analysis

The surface electronic states of the fresh, S1-poisoned, and S2-poisoned catalysts were analyzed by XPS, and the corresponding S 2p and V 2p spectra are shown in Fig. 8. The surface atomic ratios are listed in Table 1. XPS is a surface-sensitive spectroscopic technique that facilitates the quantification of the surface S content of catalysts during poisoning [39]. As shown in Fig. 8(a) and (b) and Table 1, the sulfur concentration intensity significantly increased in V/Ti, while that in VWS_2/Ti(H) remained consistent.

V 2p spectra in Fig. 8(c) and (d) could be divided into V^{4+} (515.2–515.6 eV) and V^{5+} (516.5–516.9 eV) [40]. The ratio of the V^{4+} species increased in all catalysts as S1- and S2-poisoning progressed, as

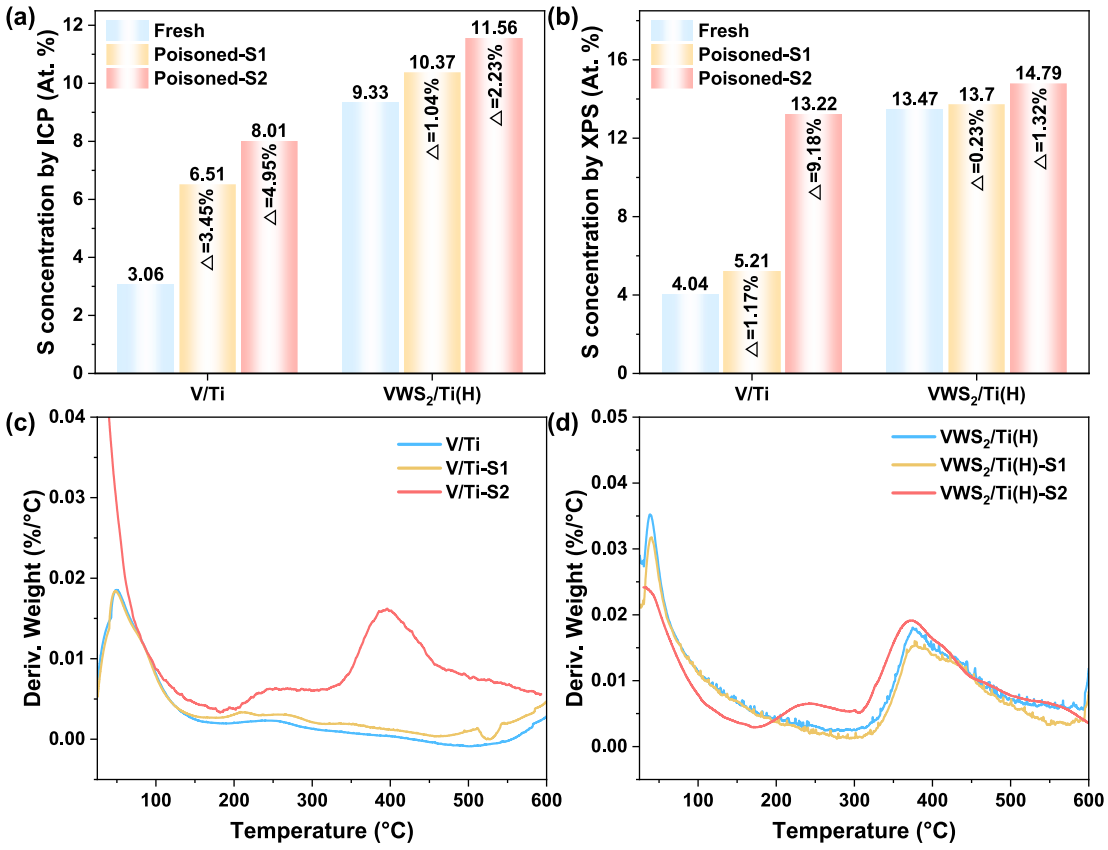

Fig. 9. Sulfur concentrations of fresh, S1-poisoned, and S2-poisoned determined using ICP-OES (a) and XPS (b) for V/Ti and VWS_2/Ti(H). Derivative weight-temperature curves of fresh, S1-poisoned, and S2-poisoned catalysts for V/Ti (c) and VWS_2/Ti(H) (d), and the corresponding TGA curves for each catalyst are presented in Fig. S21.

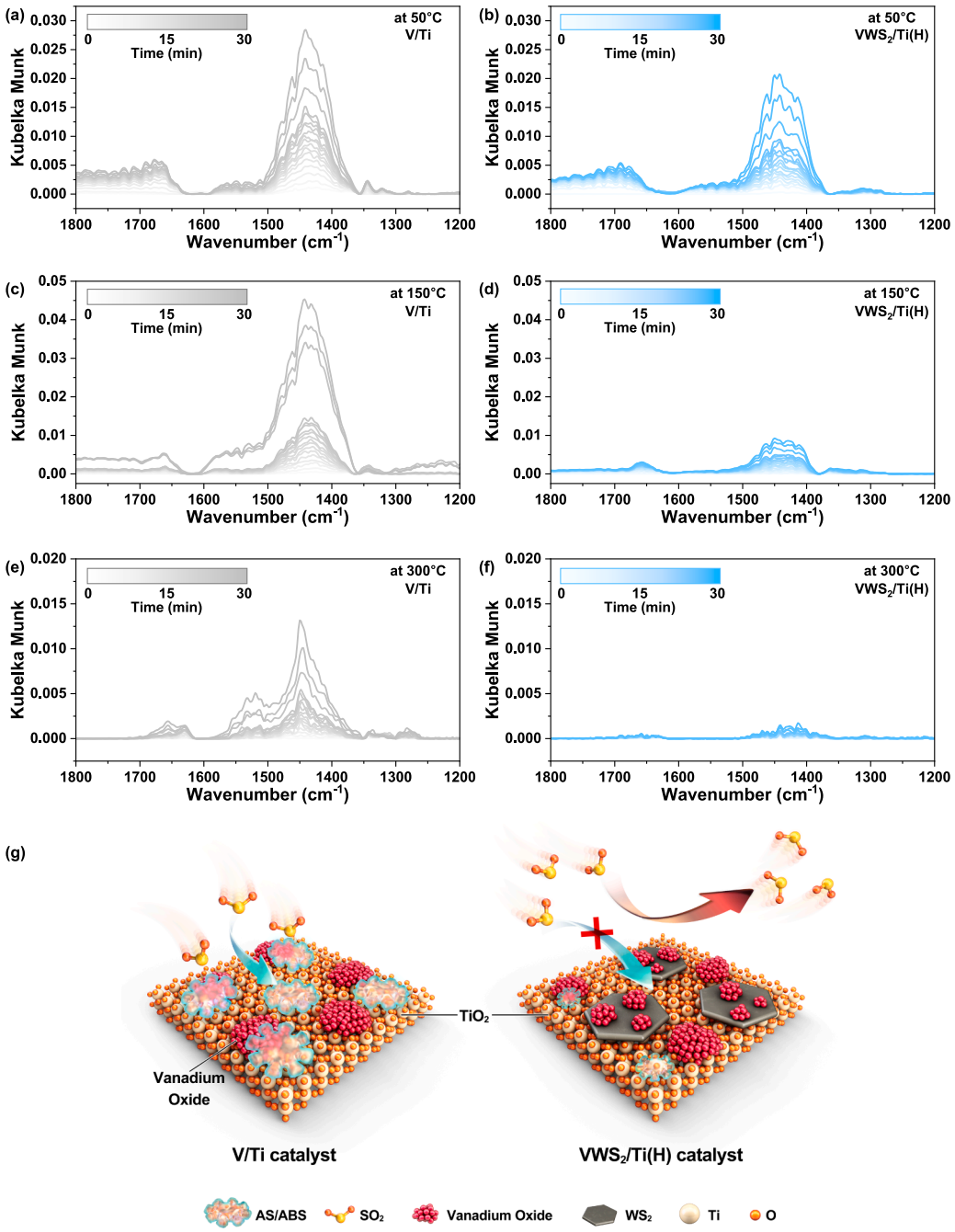

Fig. 10. In-situ DRIFTS spectra of V/Ti and VWS_2/Ti(H) at 50 (a,b), 150 (c,d), and 300 °C (e,f) following a 30-min SO_2-exposure test. The reaction conditions were: 300 ppm SO_2 + 5 % O_2, which was balanced with N_2. (g) Schematic diagram depicting the influence of WS_2 on SO_2 adsorption.

presented in Table 1. The oxidation of SO_2 to SO_3 was essential for SO_2 adsorption and the formation of sulfate species [41]. The oxidation of SO_2 to SO_3 is facilitated by vanadium, undergoing a redox cycle in which V^{5+} is reduced to V^{4+} [42,43]. The ratio of the V^{4+} species increased significantly more in V/Ti than in VWS_2/Ti(H) when poisoned with S2 condition. These results suggest that V/Ti adsorbs more SO_2 compared to VWS_2/Ti(H), leading to an increased conversion of SO_2 to SO_3. The sulfur and V surface atomic ratio results indicated that SO_2 adsorption was inhibited more in VWS_2/Ti(H) than in V/Ti

3.6.2. *Quantitative analysis of sulfur*

To further investigate the generation of sulfate byproducts between SO_2 and the catalysts during SO_2-poisoning, ICP-OES and XPS studies were performed to quantitatively compare the sulfur contents of V/Ti and VWS_2/Ti(H) before and after poisoning. As shown in Fig. 9(a) and (b), both the ICP and XPS results indicated a smaller increase in the S concentration in VWS_2/Ti(H) compared with that in V/Ti, confirming the superior SO_2 adsorption inhibition of VWS_2/Ti(H). This result was more pronounced in the XPS analysis, which could only detect the atomic concentration on the surface of the catalyst, than in the ICP analysis, which measured the overall atomic concentration in the bulk catalyst, indicating that the V/Ti surface generated significantly more sulfate. FT-IR surface analysis further confirms these results (Fig. S22) [44].

The derivative weight–temperature curves of the catalysts before and after the SO_2-poisoning test were compared and are presented in Fig. 9 (c) and (d). V/Ti-S1 and VWS_2/Ti(H)-S1 did not exhibit additional weight loss peaks compared with those of the fresh catalysts. However,

the main weight loss peak of the catalysts after the S2-poisoning occurred at approximately 240 and 400 °C, corresponding to the decomposition of AS and ABS, respectively [45,46,47]. These peaks were clearly observed in V/Ti-S2, while VWS_2/Ti(H)-S2 displayed only a peak at 240 °C and a minimal increase in the peak at 400 °C. This suggested that VWS_2/Ti(H) exhibited minimal reactivity with SO_2. This was also confirmed by the H_2-TPR results in Figs. S23(a) and (b), with the H_2-TPR profile of the fresh catalysts presented in Fig. S24. The sulfate reduction peak above 400 °C was observed in V/Ti, as confirmed by Table 1. These results demonstrated that VWS_2/Ti(H) suppressed SO_2 adsorption, thereby inhibiting the formation of AS and ABS species, which strongly supported the conclusions drawn in the previous sections [15,48].

3.7. In-situ DRIFTS: SO_2 adsorption study

The in-situ DRIFTS spectra of SO_2 adsorption on V/Ti and VWS_2/Ti(H) at various temperatures were collected to explore the adsorption properties of the catalysts, as shown in Fig. 10. The strong band at 1442 cm^{-1} was related to the surface sulfate species (S═O) [20,49], and the peaks corresponding to the surface basic hydroxyl group species (SO_2–OH) at 1664 cm^{-1} rapidly escalated on the V/Ti catalysts [8,50], with the intensity significantly exceeding the surface sulfate peaks on VWS_2/Ti(H). This observation indicated the weak adsorption of SO_2 on the VWS_2/Ti(H) surface. This became more apparent with increasing temperature because of the exothermic adsorption reactions. Furthermore, a broad band at 1531 cm^{-1}, which was assigned to the SO_3^{2-} species, was observed only for the V/Ti catalyst. These results provide additional confirmation of the protective effect of WS_2 on the VWS_2/Ti(H) catalyst surface against SO_2-poisoning by suppressing SO_2 adsorption, as depicted in Fig. 10(g).

4. Conclusion

This study presented a simple and effective strategy for enhancing the activity and stability of V-based NH_3-SCR catalysts against SO_2-poisoning. Notably, the synthesis process of the commercial VW/Ti catalyst remained unchanged, with only the promoter material requiring change. The loading of WS_2 onto the V-based catalyst resulted in the presence of a stable sulfide on the catalyst surface, which suppressed sulfur adsorption, thereby enhancing the SO_2 resistance. In addition, the high NH_3 adsorption capacity of WS_2 promoted the reaction, and hydrogen annealing was applied to increase the number of active sites on the basal plane, thereby improving the catalytic activity. While all catalysts followed the E–R and L–H mechanisms, the SO_2-poisoned V/Ti catalyst exhibited a significantly reduced NH_3 adsorption capacity. Furthermore, this catalyst primarily underwent physical adsorption rather than chemisorption during NH_3 adsorption, making it difficult for it to react with NO, leading to a decrease in activity. Conversely, the VWS_2/Ti(H) catalyst did not exhibit a decreased activity because the presence of WS_2 effectively inhibited SO_2 adsorption and oxidation, allowing easy adsorption and reaction of the NH_3 and NO species. The promoter did not adsorb SO_2 in place of the main catalyst material; rather it inhibited SO_2 adsorption, thereby significantly improving the SO_2 resistance stability. This study provides a new approach for designing V-based low-temperature NH_3-SCR catalysts with improved tolerances to SO_2-poisoning.

CRediT authorship contribution statement

Donghyeok Kim: Writing – original draft, Investigation, Formal analysis, Data curation, Conceptualization. **Myeung-Jin Lee:** Methodology. **Yejin Choi:** Data curation. **Jongkyoung Kim:** Writing – review & editing. **Bora Jeong:** Validation. **Bora Ye:** Validation. **Seungho Cho:** Writing – review & editing, Validation, Supervision. **Hong-Dae Kim:** Writing – review & editing, Supervision, Funding acquisition, Conceptualization.

Declaration of competing interest

The authors declare that they have no known competing financial interests or personal relationships that could have appeared to influence the work reported in this paper.

Acknowledgments

This study was supported by National Research Foundation of Korea (Grant number RS-2023-00281706).

Appendix A. Supplementary data

Supplementary data to this article can be found online at https://doi.org/10.1016/j.cej.2025.160191.

Data availability

Data will be made available on request.

References

[1] Z. Shi, Q. Peng, J. E, B. Xie, J. Wei, R. Yin, G. Fu, Mechanism, performance and modification methods for NH_3-SCR catalysts: a review, Fuel 331 (2023) 125885, https://doi.org/10.1016/j.fuel.2022.125885.
[2] B. Ye, B. Jeong, M.J. Lee, T.H. Kim, S.S. Park, J. Jung, S. Lee, H.D. Kim, Recent trends in vanadium-based SCR catalysts for NOx reduction in industrial applications: stationary sources, Nano Converg. 9 (2022) 51, https://doi.org/10.1186/s40580-022-00341-7.
[3] Y. Yin, B. Luo, K. Li, B.M. Moskowitz, B. Mosevitzky Lis, I.E. Wachs, M. Zhu, Y. Sun, T. Zhu, X. Li, Plasma-assisted manipulation of vanadia nanoclusters for efficient selective catalytic reduction of NO_x, Nat Commun. 15 (2024) 3592, https://doi.org/10.1038/s41467-024-47878-1.
[4] Y. Li, T. Zhang, X. Niu, Y. Zhu, Vanadium-based catalysts for selective catalytic reduction of NOx with ammonia: synthesis, poisoning mechanism, regeneration methods and research prospects, Fuel 365 (2024) 131184, https://doi.org/10.1016/j.fuel.2024.131184.
[5] K. Guo, J. Ji, W. Song, J. Sun, C. Tang, L. Dong, Conquering ammonium bisulfate poison over low-temperature NH_3-SCR catalysts: a critical review, Appl. Catal. B Environ. 297 (2021) 120388, https://doi.org/10.1016/j.apcatb.2021.120388.
[6] Y. Li, H. Li, Z. Wang, G. Li, W. Liu, J. Ji, H. Peng, Three-dimensionally ordered macroporous CeZrVOx catalyst with remarkable NH_3-SCR performance and SO_2 tolerance: key roles of the morphology and highly dispersed V species, Appl. Catal. B Environ. Energy 357 (2024) 124329, https://doi.org/10.1016/j.apcatb.2024.124329.
[7] Y. Cai, B. Zhang, H. Yu, X. Ji, J. Sun, X. Wang, Q. Qian, L. Li, A. Liu, W. Tan, F. Gao, L. Dong, Shielding ceria based catalysts from SO_2 poisoning in NH_3-SCR reaction: modification effect of acid metal oxides, Appl. Catal. B Environ. 342 (2024) 124329, https://doi.org/10.1016/j.apcatb.2023.123424.
[8] Y. Huo, K. Liu, J. Liu, H. He, Effects of SO_2 on standard and fast SCR over CeWO : a quantitative study of the reaction pathway and active sites, Appl. Catal. B Environ. 301 (2022) 120784, https://doi.org/10.1016/j.apcatb.2021.120784.
[9] Y. Xu, X. Wu, Q. Lin, J. Hu, R. Ran, D. Weng, SO_2 promoted V_2O_5-MoO_3/TiO_2 catalyst for NH_3-SCR of NO at low temperatures, Appl. Catal. A Gen. 570 (2019) 42–50, https://doi.org/10.1016/j.apcata.2018.10.040.
[10] M.G. Jung, J.H. Shin, D.W. Kwon, S.C. Hong, Promotional effects of Me (Sb, La, Ce, Mo) additives on the NH_3-SCR activity and SO_2 durability of V_2O_5-WO_3/TiO_2 catalysts, Process Saf. Environ. Prot. 183 (2024) 911–924, https://doi.org/10.1016/j.psep.2024.01.044.
[11] Y. Yu, W. Tan, D. An, X. Wang, A. Liu, W. Zou, C. Tang, C. Ge, Q. Tong, J. Sun, L. Dong, Insight into the SO_2 resistance mechanism on γ-Fe_2O_3 catalyst in NH_3-SCR reaction: a collaborated experimental and DFT study, Appl. Catal. B Environ. 281 (2021) 119544, https://doi.org/10.1016/j.apcatb.2020.119544.
[12] J. Song, X. Sun, G. Zhang, S. Cheng, Y. Xu, Y. Jiang, Recent advances in improving SO_2 resistance of Ce-based catalysts for NH_3-SCR: mechanisms and strategies, Mol. Catal. 564 (2024) 114347, https://doi.org/10.1016/j.mcat.2024.114347.
[13] Z. Xu, J. Xiong, Y. Li, J. Guo, B. Wang, T. Zhu, Mechanism of ammonium bisulfate deposition on V1M5/Ti catalysts with synergistic effects of V and M (M = Ce Co, Fe, and Mn) in low-temperature NH3-SCR, Catal. Sci. Technol. 14 (2024) 1931–1941, https://doi.org/10.1039/d3cy01801f.
[14] W. Tan, A. Liu, S. Xie, Y. Yan, T.E. Shaw, Y. Pu, K. Guo, L. Li, S. Yu, F. Gao, F. Liu, L. Dong, Ce-Si mixed oxide: a high sulfur resistant catalyst in the NH_3-SCR reaction through the mechanism-enhanced process, Environ. Sci. Technol. 55 (2021) 4017–4026, https://doi.org/10.1021/acs.est.0c08410.
[15] S. Li, F. Wang, D. Ng, Q. Shi, T.J. Raeber, S. James, B. Shen, Z. Xie, A facile $MnSO_4$ surface coated NiMnFeOx catalyst with enhanced SO_2 resistance for SCR reaction: a

dual-protection mechanism, Appl. Catal. B Environ. 342 (2024) 123441, https://doi.org/10.1016/j.apcatb.2023.123441.
[16] X. Huang, N. Fang, S. Wu, F. Dong, Y. Chu, Z. Tang, Interfacial confinement effect induced by pre-sulfurization for promoting SO_2 tolerance of MnFe-TOS catalyst in low temperature NH_3-SCR reaction, Appl. Catal. B Environ. 343 (2024) 123518, https://doi.org/10.1016/j.apcatb.2023.123518.
[17] C. Li, D. Sang, S. Ge, L. Zou, Q. Wang, Recent excellent optoelectronic applications based on two-dimensional WS_2 nanomaterials: a review, Molecules 29 (2024) 3341, https://doi.org/10.3390/molecules29143341.
[18] E.H. Hill, Layered 2D material heterostructures – a colloidal perspective, J. Mater. Chem. C 12 (2024) 11285–11318, https://doi.org/10.1039/d4tc01102c.
[19] F. Chen, H. Guo, L. Zhao, Y. Zhu, X. Wang, Y. Chu, S. Li, X. Guo, Defect engineering can enhance the electrochemical performance of WS_2 for thermal batteries, J. Electrochem. Soc. 168 (2021) 103507, https://doi.org/10.1149/1945-7111/ac2ebe.
[20] D.W. Kwon, D.H. Kim, S. Lee, J. Kim, H.P. Ha, A dual catalytic strategy by the nature of the functionalization effect as well as active species on vanadium-based catalyst for enhanced low temperature SCR, Appl. Catal. B Environ. 289 (2021) 120032, https://doi.org/10.1016/j.apcatb.2021.120032.
[21] X. Ding, T. Liu, S. Ahmed, N. Bao, J. Ding, J. Yi, Enhanced ferromagnetism in WS2 via defect engineering, J. Alloys Compd. 772 (2019) 740–744, https://doi.org/10.1016/j.jallcom.2018.09.088.
[22] Y. Jin, J. Li, K. Fan, Y. Chen, Y. Yang, X. Liu, The nature of synergy effects between VO and TiO_2 in low temperature NH_3-SCR reaction, J. Environ. Chem. Eng. 12 (2024) 113689, https://doi.org/10.1016/j.jece.2024.113689.
[23] P. Zhou, Q. Xu, H. Li, Y. Wang, B. Yan, Y. Zhou, J. Chen, J. Zhang, K. Wang, Fabrication of two-dimensional lateral heterostructures of WS_2 /WO_3 ·H_2O through selective oxidation of monolayer WS_2, Angew. Chem. Int. Ed. 54 (2015) 15226–15230, https://doi.org/10.1002/anie.201508216.
[24] G. He, Z. Lian, Y. Yu, Y. Yang, K. Liu, X. Shi, Z. Yan, W. Shan, H. He, Polymeric vanadyl species determine the low-temperature activity of V-based catalysts for the SCR of NO_x with NH_3, Sci. Adv. 4 (2018) eaau4637, https://doi.org/10.1126/sciadv.aau4637.
[25] K.H. Hwang, N. Park, H. Lee, K.-M. Lee, S.W. Jeon, H.S. Kim, Y. Lee, T.J. Kim, W. B. Lee, D.H. Kim, Mechanochemical localization of vanadia on titania to prepare a highly sulfur-resistant catalyst for low-temperature NH_3-SCR, Appl. Catal. B Environ. 324 (2023) 122290, https://doi.org/10.1016/j.apcatb.2022.122290.
[26] X. Zhao, Y. Yan, L. Mao, M. Fu, H. Zhao, L. Sun, Y. Xiao, G. Dong, A relationship between the V^{4+}/V^{5+} ratio and the surface dispersion, surface acidity, and redox performance of V_2O_5-WO_3/TiO_2 SCR catalysts, RSC Adv. 8 (2018) 31081–31093, https://doi.org/10.1039/c8ra02857e.
[27] A. Nellessen, A. Schaefer, A. Martinelli, A. Raj, A. Newman, P.-A. Carlsson, Impact of vanadium loading and thermal aging on the surface properties of titania-supported vanadium oxide, J. Phys. Chem. C 128 (2024) 2894–2908, https://doi.org/10.1021/acs.jpcc.3c08081.
[28] M. Jiang, Z. Yan, Y. Zhang, C. Zhang, C. Chang, M. Xiao, L. Ruan, Y. Yan, Y. Yu, H. He, Simultaneous modification of redox and acidic properties of FeOx catalysts derived from MIL-100(Fe) via HPW incorporation for NH_3-SCR, Appl. Catal. B Environ. Energy 358 (2024) 124416, https://doi.org/10.1016/j.apcatb.2024.124416.
[29] X. Yi, J. Wang, Y. Liu, Y. Chen, J. Chen, Promotional effect of Fe and Ce co-doping on a V_2O_5–WO_3/TiO_2 catalyst for SCR of NOx with high K and Pb resistance, Catal. Sci. Technol. 12 (2022) 4169–4180, https://doi.org/10.1039/d2cy00818a.
[30] J. Wang, Z. Yan, L. Liu, Y. Chen, Z. Zhang, X. Wang, In situ DRIFTS investigation on the SCR of NO with NH_3 over V_2O_5 catalyst supported by activated semi-coke, Appl. Surf. Sci. 313 (2014) 660–669, https://doi.org/10.1016/j.apsusc.2014.06.043.
[31] R. Wu, N. Zhang, L. Li, H. He, L. Song, W. Qiu, DRIFT study on promotion effect of the keggin structure over V_2O_5-MoO_3/TiO_2 catalysts for low temperature NH_3-SCR reaction, Catalysts 8 (2018) 143, https://doi.org/10.3390/catal8040143.
[32] Y. Zhang, X. Yue, T. Huang, K. Shen, B. Lu, In Situ DRIFTS studies of NH_3-SCR mechanism over V_2O_5-CeO_2/TiO_2-ZrO_2 catalysts for selective catalytic reduction of NO_x, Materials. 11 (2018) 1307, https://doi.org/10.3390/ma11081307.
[33] X. Wang, Q. Cong, L. Chen, Y. Shi, Y. Shi, S. Li, W. Li, The alkali resistance of CuNbTi catalyst for selective reduction of NO by NH_3: a comparative investigation with VWTi catalyst, Appl. Catal. B Environ. 246 (2019) 166–179, https://doi.org/10.1016/j.apcatb.2019.01.049.
[34] Q. Yan, J. Xiao, R. Gui, Z. Chen, Y. Wang, Y. Li, T. Zhu, Q. Wang, Y. Xin, Insights into enhancement of NH_3-SCR activity and N_2 selectivity of LDHs-derived NiMnAlOx catalysts: combination of experiments and DFT calculations, Appl. Catal. B Environ. 343 (2024) 123489, https://doi.org/10.1016/j.apcatb.2023.123489.
[35] Y. Shen, Z. Wang, S. Ge, L. Wang, W. Zhan, Q. Dai, Y. Guo, Y. Guo, A. Wang, Revealing the mechanisms of NH_3 adsorption and reactions in catalytic NOx reduction over Cux/CHA zeolites by in situ DRIFTS spectroscopy, Appl. Catal. B Environ. Energy 353 (2024) 124094, https://doi.org/10.1016/j.apcatb.2024.124094.
[36] J. Ji, N. Gao, W. Song, Y. Tang, Y. Cai, L. Han, L. Cheng, J. Sun, S. Ma, Y. Chu, C. Tang, L. Dong, Understanding the temperature-dependent H_2O promotion effect on SO_2 resistance of MnO -CeO_2 catalyst for SCR denitration, Appl. Catal. B Environ. 324 (2023) 122263, https://doi.org/10.1016/j.apcatb.2022.122263.
[37] L. Arnarson, H. Falsig, S.B. Rasmussen, J.V. Lauritsen, P.G. Moses, The reaction mechanism for the SCR process on monomer V^{5+} sites and the effect of modified Bronsted acidity, Phys. Chem. Chem. Phys. 18 (2016) 17071–17080, https://doi.org/10.1039/c6cp02274j.
[38] F. Gao, N.M. Washton, Y. Wang, M. Kollár, J. Szanyi, C.H.F. Peden, Effects of Si/Al ratio on Cu/SSZ-13 NH_3-SCR catalysts: implications for the active Cu species and the roles of Brønsted acidity, J. Catal. 331 (2015) 25–38, https://doi.org/10.1016/j.jcat.2015.08.004.
[39] C. Chen, Y. Wang, J. Li, F. Tian, W. Chen, C. Feng, Y. Pan, Y. Liu, In situ construction of heteroatom F-doped Mn_3O_4 spinel catalysts with robust activity and SO_2 resistance for NH_3-SCR at low temperature, Appl. Catal. B Environ. 338 (2023) 123086, https://doi.org/10.1016/j.apcatb.2023.123086.
[40] J.-K. Lai, N.R. Jaegers, B.M. Lis, M. Guo, M.E. Ford, E. Walter, Y. Wang, J.Z. Hu, I. E. Wachs, Structure–activity relationships of hydrothermally aged titania-supported vanadium–tungsten oxide catalysts for SCR of NOx emissions with NH_3, ACS Catal. 11 (2021) 12096–12111, https://doi.org/10.1021/acscatal.1c02130.
[41] J. Lu, Z. Zhou, H. Zhang, Z. Yang, Influenced factors study and evaluation for SO_2/SO_3 conversion rate in SCR process, Fuel 245 (2019) 528–533, https://doi.org/10.1016/j.fuel.2019.02.077.
[42] Y. Li, J. Xiong, Y. Lin, J. Guo, T. Zhu, Distribution of SO_2 Oxidation Products in the SCR of NO over V_2O_5/TiO_2 Catalysts at Different Temperatures, Ind. Eng. Chem. Res. 59 (2020) 5177–5185, https://doi.org/10.1021/acs.iecr.9b05271.
[43] H. Kamata, H. Ohara, K. Takahashi, A. Yukimura, Y. Seo, SO_2 oxidation over the V_2O_5/TiO_2 SCR catalyst, Catal. Lett. 73 (2001) 79–83, https://doi.org/10.1023/A:1009065030750.
[44] L. Zhu, Z. Zhong, J. Xue, Y. Xu, C. Wang, L. Wang, NH_3-SCR performance and the resistance to SO_2 for Nb doped vanadium based catalyst at low temperatures, J. Environ. Sci. (china) 65 (2018) 306–316, https://doi.org/10.1016/j.jes.2017.06.033.
[45] Y. Ni, Y. Rong, X. Yu, S. Huang, X. Xue, H. Zhou, Experimental study on the effects of reheat temperatures on the ammonium bisulfate and ash blend deposition, Fuel 324 (2022) 124719, https://doi.org/10.1016/j.fuel.2022.124719.
[46] A. Sanna, J. Gaubert, M.M. Maroto-Valer, Alternative regeneration of chemicals employed in mineral carbonation towards technology cost reduction, Chem. Eng. J. 306 (2016) 1049–1057, https://doi.org/10.1016/j.cej.2016.08.039.
[47] Y. Wang, W. Yi, J. Yu, J. Zeng, H. Chang, Novel methods for assessing the SO_2 poisoning effect and thermal regeneration possibility of MO_x-WO_3/TiO_2 (M = Fe, Mn, Cu, and V) catalysts for NH_3-SCR, Environ. Sci. Technol. 54 (2020) 12612–12620, https://doi.org/10.1021/acs.est.0c02840.
[48] W. Zhang, G. Liu, J. Jiang, Y. Tan, Q. Wang, C. Gong, D. Shen, C. Wu, Sulfation effect of Ce/TiO_2 catalyst for the selective catalytic reduction of NO_x with NH_3: mechanism and kinetic studies, RSC Adv. 9 (2019) 32110–32120, https://doi.org/10.1039/c9ra06985b.
[49] V. de Souza Bonfim, R. Barbosa de Castilho, L. Baptista, S. Pilling, SO_3 formation from the X-ray photolysis of SO_2 astrophysical ice analogues: FTIR spectroscopy and thermodynamic investigations, Phys. Chem. Chem. Phys. 19 (2017) 26906–26917, https://doi.org/10.1039/c7cp03679e.
[50] S. Han, Q. Ye, Q. Gao, H. Dai, Improved SO2 tolerance of Cu-SAPO-18 by Ce-doping in the selective catalytic reduction of NO with NH_3, Catalysts 10 (2020), https://doi.org/10.3390/catal10070783.